PERMEABILITY OF LIMESTONE-DOLOMITE COMPOSITE FRACTURE SURFACES

by

PETER JOHN VAN DE REEP

A THESIS SUBMITTED IN PARTIAL FULFILLMENT OF
THE REQUIREMENTS FOR THE DEGREE OF

BACHELOR OF SCIENCE (HONOURS)

in

THE FACULTY OF SCIENCE

Geological Sciences

This thesis conforms to the required standard

……
Supervisor

THE UNIVERSITY OF BRITISH COLUMBIA

(Vancouver)

MARCH 2009

TABLE OF CONTENTS

LIST OF FIGURES

LIST OF TABLES

ABSTRACT

The transport properties of fault zones are critically important in predicting subsurface fluid behavior in deformed rocks and understanding fold and thrust belts. Limestone-dolomite composite rocks are common components of fold and thrust belts and are also productive reservoir rocks for hydrocarbons. This study develops a methodology for measuring the permeability of experimentally induced fracture surfaces in limestone-dolomite composite rocks. Cores of rocks from the Mount Head Formation and the Fairholme Group of southern Alberta were deformed at a confining pressure of 25 MPa in a triaxial rock press. Fluid ports were drilled in the deformed cores to ensure direct fluid access to the fracture surface. The transient pulse decay method was used to determine the permeability of the fractures. Experimental difficulties resulted in only two permeabilities being derived from experimentation. Modeling of the transient pulse decay for the fracture surfaces shows permeabilities of $4 \cdot 10^{-17}$ m^2 for predominantly dolomite and $8 \cdot 10^{-17}$ m^2 for dolomitic limestone. Lower permeability in the dolomite end member is thought to be due to very fine comminution in the fracture gouge caused by highly focused strain with little distributed strain outside of the fracture itself. Increasing heterogeneity in a rock increases the distributed strain, causing an increase in permeability. This study serves as an initial development in the ability to measure the permeability of fracture surfaces. Increasing precision and accuracy of measurements is expected with further research.

INTRODUCTION

The creation and destruction of permeability during faulting is of critical importance to the understanding of fault zone evolution. Transport properties of fault zone rocks vary, depending on a number of factors, including porosity, mineralogy and the extent of deformation. Permeability is valued in the petroleum industry since it is essential for the production of hydrocarbons. This permeability may be natural or hydrofracturing techniques may be used to artificially generate permeability in a reservoir. Fault zone permeability is not always desired, for example, cap rocks for hydrocarbon reservoirs with excessive permeability may result in lower than expected production levels as fluids are lost. In addition, the interpretation of fold and thrust belts and other highly deformed regions can be assisted by an understanding of permeability and the nature of fluids flowing through fault zones.

Laboratory measurements of permeability along experimentally induced fault zones has been extensively investigated for clay-rich fault zones (Faulkner & Rutter, 2000; Crawford, et al. 2008) and work has been done on pure quartz fault zones (Giger, 2007). Few experiments have been performed on carbonate rocks, despite being being recognied as a significant reservoir rocks for hydrocarbons (Ehrenberg et al., 2006) as well as hosting the thrust faults responsible for seismic activity in Italy (Monaco et al., 1996; Pace et al., 2002). Permeability testing on fault gouges and other fault related rocks is a technically challenging endeavour due to the very low permeabilities of fine grained gouge material generated during a triaxial deformation experiment. Techniques such as the pore pressure oscillation method (Fischer, 1992) and the transient pulse decay method (Brace et al., 1968) have been developed to address the issues of determining very low permeabilities.

This research aims to develop a technique to measure the permeability of experimentally induced fault zones in limestone-dolomite composite rocks. The methodology described below will provide a starting point for future research performed at the facilities used for the experiments. Results for the permeability of the sample suite can be considered an initial foray into characterizing carbonate fault zone fluid transport properties.

Previous Work

Permeability of low porosity, “tight” rocks has been a challenging property to properly characterize. Traditional methods of measuring permeability using steady state fluid flow through rock are not effective for rocks with low permeability such as granites, shales and tight carbonates. The first technique developed to measure very low permeabilities was the transient pulse decay method developed for crystalline rocks (Brace et al., 1968). Transient pulse decay experiments assume that flow within the sample obeys Darcy’s Law.

Using this relationship along with known parameters of the system, such as the volume of the upper and lower fluid reservoirs as well as fluid properties such as viscosity and fluid compressibility, permeability can be determined. Pressure in the isolated upper fluid reservoir was increased a small amount (1 - 2 megapascals) and released to the sample. The decay curve of this pressure transient was used to calculate permeability by graphically comparing it to predicted theoretical behavior. Transient decay times were reduced to under 10 seconds at porosities of around 1%, rendering the method ineffective for porous rocks. The mathematical model for this experiment is described below.

Due to the relative simplicity of the methods outlined by Brace et al. (1968), numerous studies have made improvements on the original experiment. Graphical methods were joined by more detailed mathematical and numerical modeling approaches (Zhang et al., 2000) as well as computerized history matching algorithms (Zeynaly-Andabily & Rahman, 1995). These newer methods typically model the specific storage of the specimen in addition to permeability, something which Brace et al. (1968) did not include in their initial research. Regardless, the simpler, original approach remains in use by researchers today.

Another technique to measure permeability, increasingly seen in the literature, is the pore pressure oscillation method (Fischer, 1992). Pore pressure oscillation determines both permeability and specific storage of a sample by analyzing the attenuation and phase shift of a controlled frequency pressure variation of the pore fluid. The experimental setup requires the addition of volumometers and computer based drivers to monitor and control the pressure

oscillations. For this reason, this approach was not used to determine permeability in this study.

METHODOLOGY

Apparatus

Rock deformation experiments were performed using the Centre for Experimental Study of the Lithosphere (CESL) Large Sample Rig (LSR) at the University of British Columbia Department of Earth and Ocean Sciences (EOS) in Vancouver, British Columbia. The LSR is a triaxial rock press capable of exerting both confining and fluid pressures on a sample. Argon is used as a confining medium (up to 100 megapascals (MPa) with the current gas booster configuration). A fluid pressure system acts independently of the confining pressure system and uses distilled water as the pore fluid. The LSR is a modified version of the rock presses in use at Texas A & M University, designed by Dr. John Logan and introduced by Austin (2003).

Cylindrical cored samples are deformed in a pressure vessel rated to 500 MPa. The pressure vessel is made of H13 hardened steel with a wall thickness of 8.26 cm. A compensating vessel and piston at the base of the main pressure vessel maintain constant vessel volume with changing confining pressure. An electric motor and gear assembly provides load through a thrust bearing and ball bearing screw to ensure axial loading of up to 200 000 pounds. The load system moves the pressure vessel at a constant displacement rate upwards towards the stationary upper plate. This displacement rate can be set using a variable motor controller. Displacement is measured with a direct current displacement transducer (DCDT) mounted between the upper stationary and lower moving plate of the rig. Load data is acquired by an external load cell mounted above the pressure vessel and sample assembly. Confining pressure is monitored using both an analog gauge and a digital pressure transducer. All data is monitored and logged in real time through LabVIEW software. The instrument sample rate is 0.375 seconds per datum.

A pore fluid pressure system is installed on the rig and is capable of independent operation from the confining pressure system. Using distilled water as the fluid, the system can apply a maximum fluid pressure of 34 MPa. An HiP 87-6-5 high pressure generator manual piston screw pump is used to generate the desired fluid pressure. A remote operated valve can be used to isolate the upper fluid reservoir from the sample and lower fluid reservoir. Pressure transducers are located both upstream and downstream from the sample to acquire fluid pressure data from both the upper and lower fluid reservoirs. Outlet valves allowing for drainage and vacuum evacuation of the system are installed on both the upper and lower reservoirs. Fluid pressure data can be monitored in real time from the LabVIEW software environment as well.

Sample Preparation

Right cylindrical cores with a length of 60 millimeters (mm) and diameter of 30 mm were used in the triaxial experiments. Each core was precision honed such that the ends were parallel within 0.0127 mm. Length and diameter of each specimen was recorded at 5 different positions for each dimension to calculate a mean measurement for the core. Specimens were visually inspected to ensure no preferential failure surfaces were present. Helium pycnometry was performed on the sample suite by Cleven (2008) to determine porosity and skeletal density. X-ray fluorescence analysis, performed by ALS Chemex, was used to determine the percentage of dolomite for each rock type in the suite.

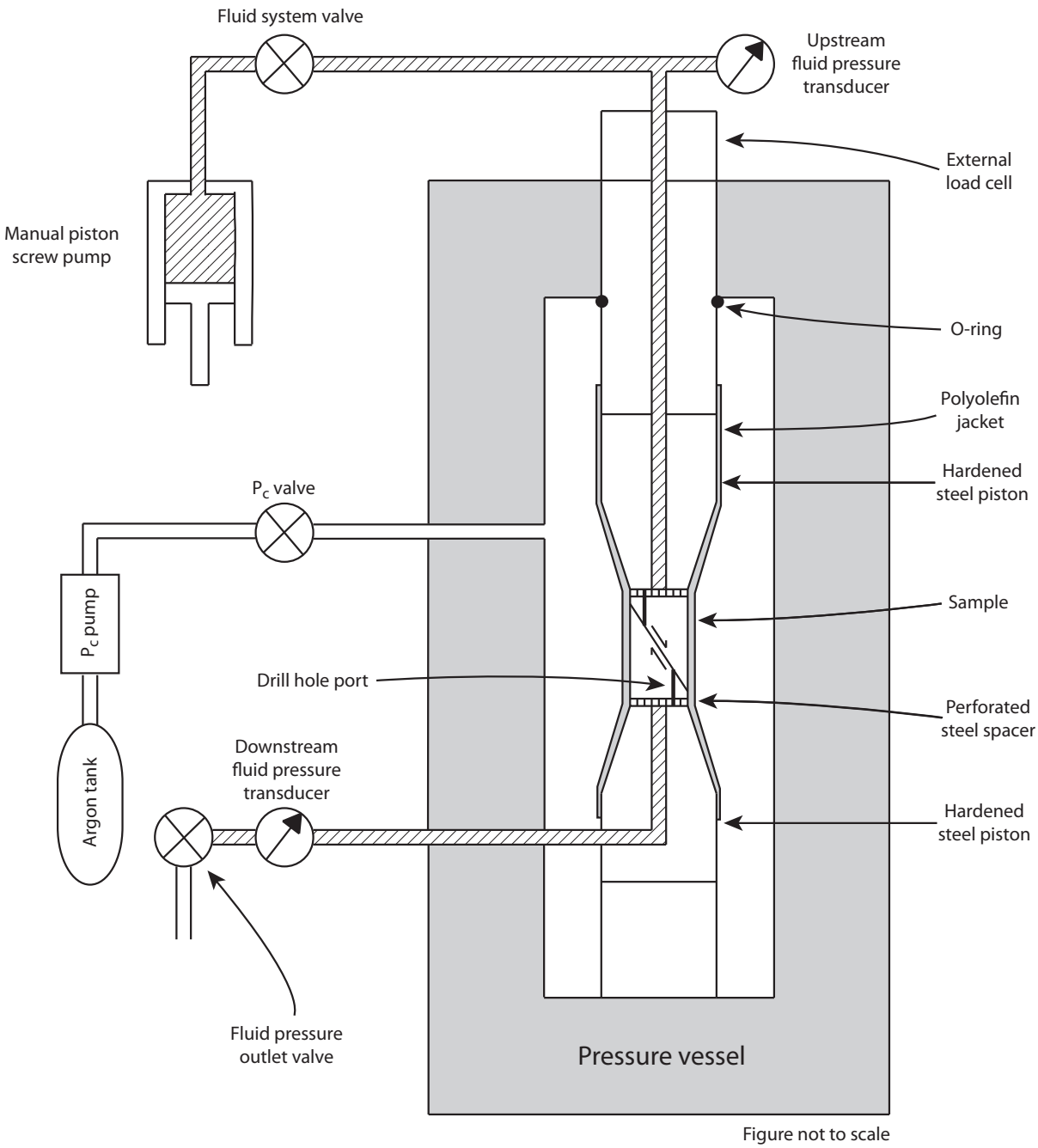

Figure 1. Pore fluid system schematic for the LSR.

Sample Assembly

A heat shrinkable polyolefin jacket was affixed to each core with Loctite Superflex Blue RTV silicone adhesive and allowed to cure for 24 hours. This seal prevented fluid flow between the sample and its jacket. Once cured, the sample was placed between appropriately sized spacers and the upper and lower piston cups. A polyolefin jacket was used to maintain axial alignment and prevent argon from permeating the sample or escaping through the pore fluid system. Nichrome steel wire seals were affixed at both ends of the sample assembly to completely isolate the sample from the confining pressure medium. At the pressure, temperature and duration of experimentation, argon does not permeate the polyolefin jackets.

Figure 2. **A.** LSR detail with sample assembly inserted and pore fluid system installed. **B.** Sample assembly detail with fractured 30 mm diameter sample, polyolefin jacket and wire seals in place.

Experimental Procedure - Rock Deformation

Samples were inserted into the LSR pressure vessel along with polycarbonate spacers to minimize the internal volume of the vessel. The vessel was sealed off with the upper nut and gland assembly. The lower seal of the pressure vessel is formed by o-ring closures at the base of the lower piston cup. Displacement between the plates was adjusted to allow for the

installation of load cell. Following this, minimal load was applied to the assembly to prevent assembly instability while pumping up the confining pressure. Transducers were reset to zero values and the confining pressure pump was tested to ensure proper working order. Confining pressure was increased to 25 MPa . The displacement motor was then activated at a rate of 0.31 cms^{-1} until failure of the sample occurred. Failure was noted both by a significant, near instantaneous drop in load and a sharp loud acoustic emission. Immediately following failure, the displacement motor was halted and the experiment was ended.

Experimental Procedure - Permeability Tests

Each core was measured and marked for precision drilling of fluid ports on each end of the sample. This port allowed for direct access of the pore fluid to the fracture surface. Each port was drilled at a distance of 7.5 mm from the outside edge of the core with the exception of rocks that featured a fracture on the end surface of the core. These cores were drilled at a distance of 5 mm towards the centre of the core, away from the fracture expression. Once drilled, the cores were allowed to soak in water for a minimum of 24 hours before experimentation to increase fluid saturation of the sample. Though vacuum impregnation of the samples with water would have increased sample saturation, the original structure of the fracture gouge, and thus permeability would have been affected. Very fine glass beads were lightly packed into each fluid port to prevent fault gouge extrusion during the experiment (Crawford et al., 2008). The sample was then assembled as described above and placed into the LSR pressure vessel. Upper and lower reservoirs of the pore fluid pressure system were connected to the assembly and a minimal axial load was applied. Both reservoirs were evacuated with a vacuum pump to eliminate all fluids remaining in the system and to ensure even release of water through the reservoirs when the system was opened.

To begin a test, confining pressure was increased to 5 MPa. Fluid pressure was then increased until the upper reservoir was full and the upper transducer was reading an increase in pressure. Fluid pressure was applied at intervals until both the upper and lower transducers were reading about 3 MPa. Depending on the sample being tested, the reservoirs could take up to an hour to equilibrate. From here, fluid pressure and confining pressure were alternately

increased to the desired experimental conditions. This was done stepwise to ensure the differential stress did not exceed the differential stress desired for the transient pulse test (in this case, 5 MPa). To conduct the transient pulse test the upper reservoir valve was closed, isolating it from the sample. Pressure was increased in the upper reservoir by 15% and the valve was opened. The fluid system was monitored through the transducers to ensure no leaks were occurring. Unfortunately, leaks and fluids bypassing the sample by flowing through the annular space between the sample and its jacket were a common occurrence.

Data Reduction

The program used to collect data for both mechanical testing and pore fluid pressure, LabVIEW, logs all data from the initiation of an experiment until the session is ended. The raw data set must therefore be reduced to remove all data unrelated to the specific experiment. Reduction for deformation experiments was done graphically in MATLAB, eliminating portions of the experiment unrelated to the loading and subsequent straining of the specimen. A Microsoft Excel spreadsheet designed and created by Cleven (2008) was used for the calculation of stress and strain from the raw displacement and load data. Pore fluid data was reduced graphically as well, with data series created and plotted for the individual transient pulse experiments. Refer to appendix for a figure of the raw data series.

Starting Material

Samples used in experimentation were collected by Cleven at various localities in the Rocky Mountains of southern Alberta. The sample suite consists of low porosity, fine grained limestones and dolostones end members as well as intermediate composites. Most of the samples were taken from the Mount Head Formation, a Mississippian unit comprised predominantly of variably dolomitized limestone and dolostone. Member units of the Mount Head selected for experimentation were the Baril Wileman and Loomis. These rocks provided both the low-dolomite content end member as well as intermediate limestone dolomite composites. Near-pure dolostones from the Devonian Fairholme Group were also selected for experiments. To minimize the effects of deformation due to pore size reduction,

rocks with low porosity were selected. Average porosity was determined using the UBC EOS helium pycnometer using a number of cores from each rock type (Table 1). X-ray fluorescence analysis was performed on the samples to determine composition (Table 2).

Table 1. Average sample porosity from helium pycnometry data (Cleven, 2008)

Rock	Porosity (%)
Loomis 3	0.5
Loomis 43	0.3
Baril Wileman 83	3.4
Fairholme C	1.6

Table 2. Normative mineralogy of experimental sample suite from XRF data (Cleven, 2008)

Rock	Silica (%)	Calcite (%)	Dolomite (%)
Loomis 3	1.14	95.71	3.15
Loomis 43	8.56	48.14	43.30
Baril Wileman 83	1.80	14.72	83.49
Fairholme C	0.78	0.61	98.60

Mathematical Model

The pulse decay method of determining permeability can be modeled with varying degrees of complexity. Initial models assumed the sample had no compressive storage. This is a reasonable assumption for most crystalline rocks, like the Westerly granite initially used for these studies. It is assumed that Darcy's Law applies for fluid flow within the sample as shown by

$$q = -\frac{kA}{\mu}\frac{\delta P}{\delta x} \tag{1}$$

where q is flow through the sample, k is permeability, A is the cross sectional area of the sample, μ is dynamic fluid viscosity, P is pressure and x is the length along the sample.

The following relationship describes one dimensional transient compressible fluid flow through a compressible medium

$$\frac{\partial^2 P}{\partial x^2} = \frac{\mu\beta}{k}\left[\frac{\beta_{\text{eff}} - \beta_s}{\beta} + \phi\left(1 - \frac{\beta_s}{\beta}\right)\right]\frac{\partial P}{\partial t} \tag{2}$$

where β is fluid compressibility, β_{eff} is the effective compressibility of the rock as a jacketed sample, β_s is the bulk compressibility of the rock's minerals, Φ is porosity and x in this case is the distance to the end of the sample. The compressibility of the pore fluid, in this study, water, is taken to be significantly greater than the compressibility of the sample. If the sample porosity is low, the above expression can be further simplified. As the rocks in this study are low porosity dolomites and limestones, the following assumptions are made

$$\frac{\beta_{\text{eff}} - \beta_s}{\beta} \approx 0 \qquad \phi(1 - \frac{\beta_s}{\beta}) \approx 0 \tag{3}$$

This results in the 1-D transient flow equation simplifying to

$$\frac{\partial^2 P}{\partial x^2} = 0 \tag{4}$$

From this, the pressure in the system can be described as having a constant gradient along the sample length which varies over time.

$$\frac{\partial P}{\partial x} = f(t) \tag{5}$$

Brace et al. (1968) used an analogy to describe the reservoir-sample system by approaching the sample as a resistor and the reservoirs as capacitors. Using this analogy, the system can be modeled to show an exponential decay in the pressure gradient over the time frame of the experiment. The upper reservoir pressure is described by7

$$(P_u - P_f) = \Delta P\left(\frac{V_l}{V_u} + V_l\right)e^{-\alpha t} \tag{6}$$

and the exponential coefficient, α, is described by

$$\alpha = \frac{kA}{\mu\beta L}\left(\frac{1}{V_u} + \frac{1}{V_l}\right) \tag{7}$$

where P_u is the upper reservoir pressure, P_f is the pressure at which the pulse decayed to, ΔP is the pressure 'pulse' at time t=0, V_l is the volume of the lower reservoir, V_u is the volume of the upper reservoir and L is the length along the sample. In this study, this length is the measured distance between the two fluid ports on either side of the core.

When the pressure decay of the upper reservoir is plotted against time, an exponential decay curve can be modeled with the exponential coefficient equal to -α. This allows for a permeability to be calculated as it is the only remaining unknown in the final equation.

Rocks with significant compressive storage however, such as shales and other high porosity sedimentary rocks, are not accurately described by the model proposed by Brace et al. which assumes the rock is highly incompressible and crystalline. These rocks are better described by the numerous improvements made in the mathematical solutions to the pulse decay experiments (eg. Hsieh et al., 1981, Kamath et al., 1992, Zeynaly-Andabily & Rahman 1995, etc.)

RESULTS

A total of 13 cores from the sample suite were used for triaxial compression experiments. Due to numerous experimental problems, only three of these cores had full permeability tests performed on them. Only the mechanical properties of the three cores subject to the entire experimental suite will be discussed. Additional mechanical analysis is available in Cleven (2008).

Mechanical Results

All samples were deformed using constant displacement rate triaxial compression experiments at 25 MPa confining pressure. The visible deformation in each sample consisted of a primary fracture surface and depending on the sample, a network of distributed cracks secondary to the primary fracture. Distributed cracks were typically synthetically oriented.

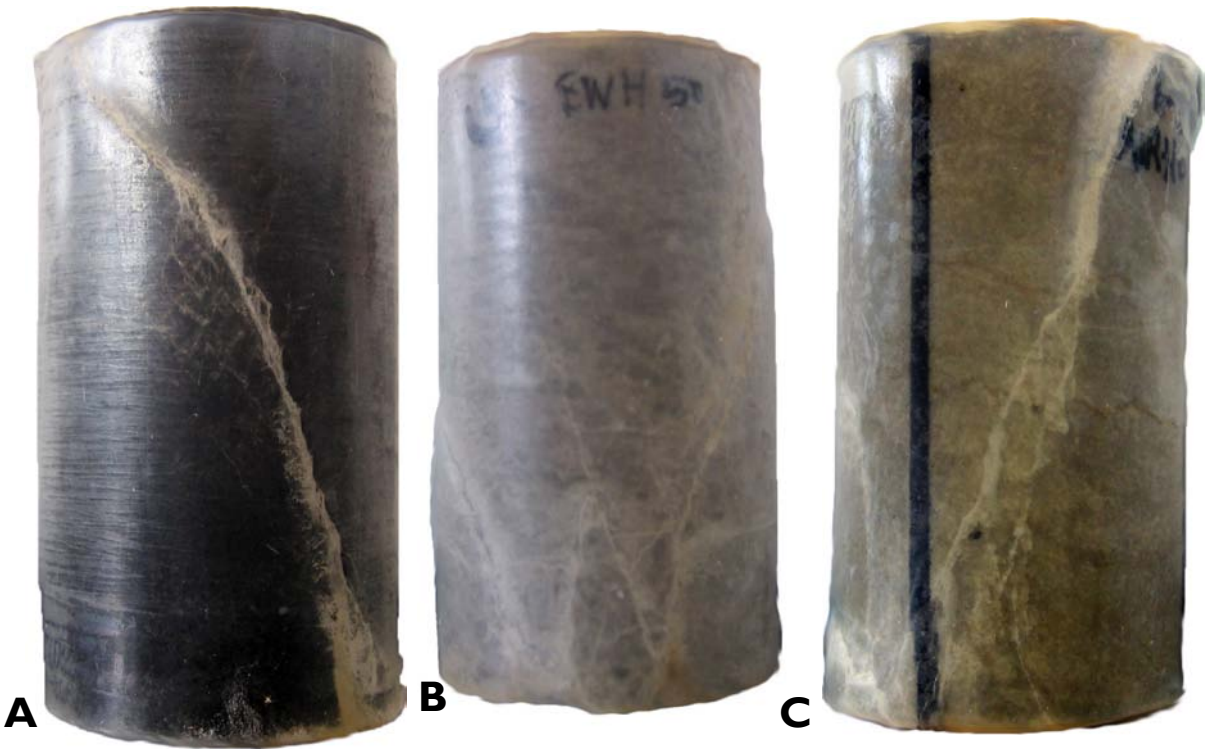

Figure 3. Deformed cores in polyolefin jacketing. **A**. Loomis 3, notice synthetic crack network just beneath primary fracture surface in center of photo. **B.** Baril Wileman 83, primary fracture runs from right to left; note conjugate fracture at bottom left. **C.** Fairholme C, distinct primary fracture only.

Stress-Strain Relationships

Stress-strain curves were plotted for each rock. The experiments show a range in peak rock strengths of 300-393 MPa (Table 3). Strength increased with increasing percentage of dolomite, as the Loomis 3 sample was the weakest rock and the Fairholme C sample was the strongest rock.

Table 3. Individual sample peak and yield strengths from triaxial compression tests.

Sample	Dolomite (%)	Yield Strength (MPa)	Yield Strain (%)	Peak Strength (MPa)	Peak Strain (%)
Loomis 3	3.15	290.9	1.83	299.7	1.95
Baril Wileman 83	83.49	324.4	2.91	334.8	3.07
Fairholme C	98.60	393.0	2.94	393.0	2.94

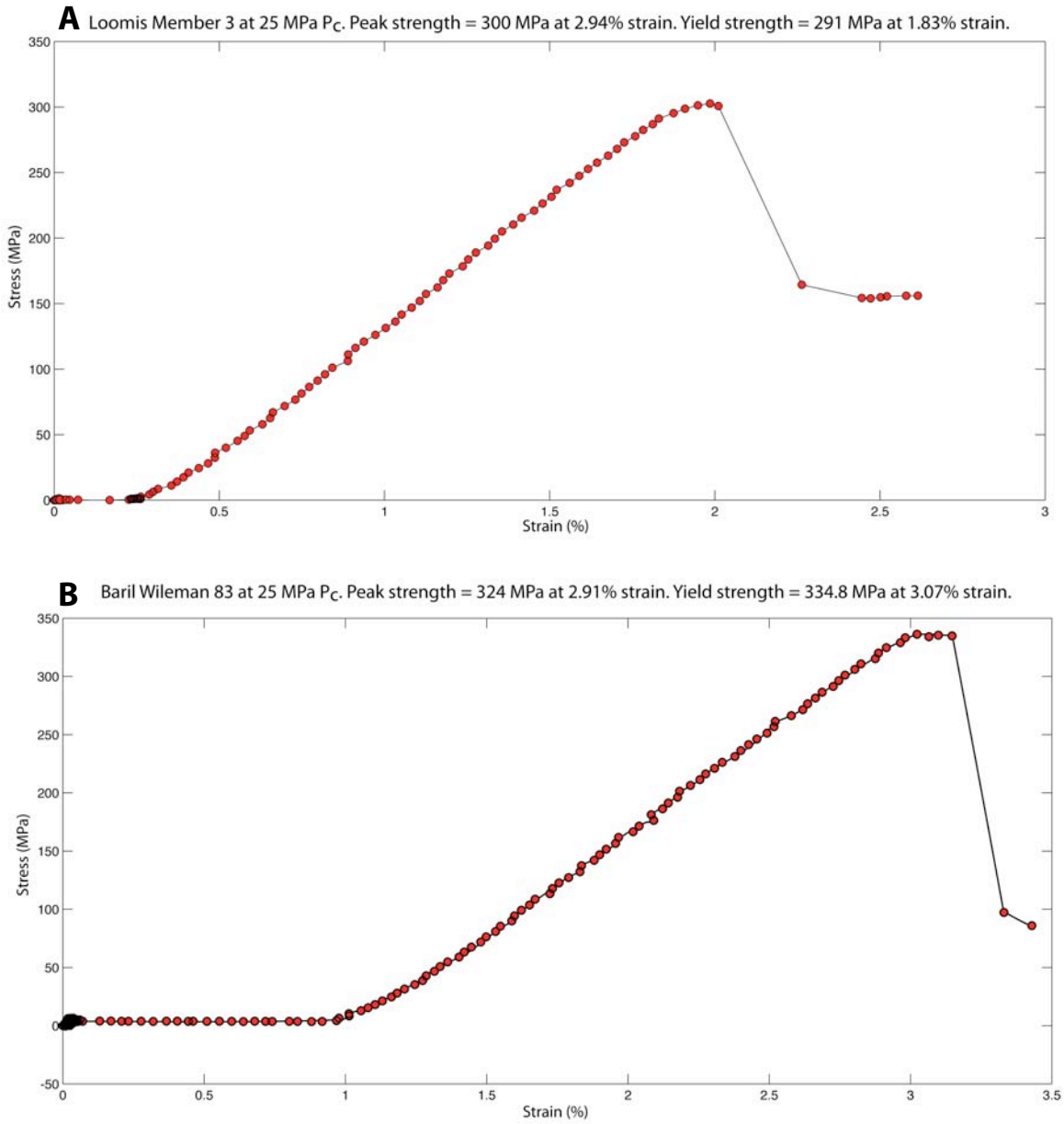

Figure 4. A. Stress-strain curve for Loomis 3 at $P_c = 25$ MPa. **B.** Stress-strain curve for Baril Wileman 83 at $P_c = 25$ MPa.

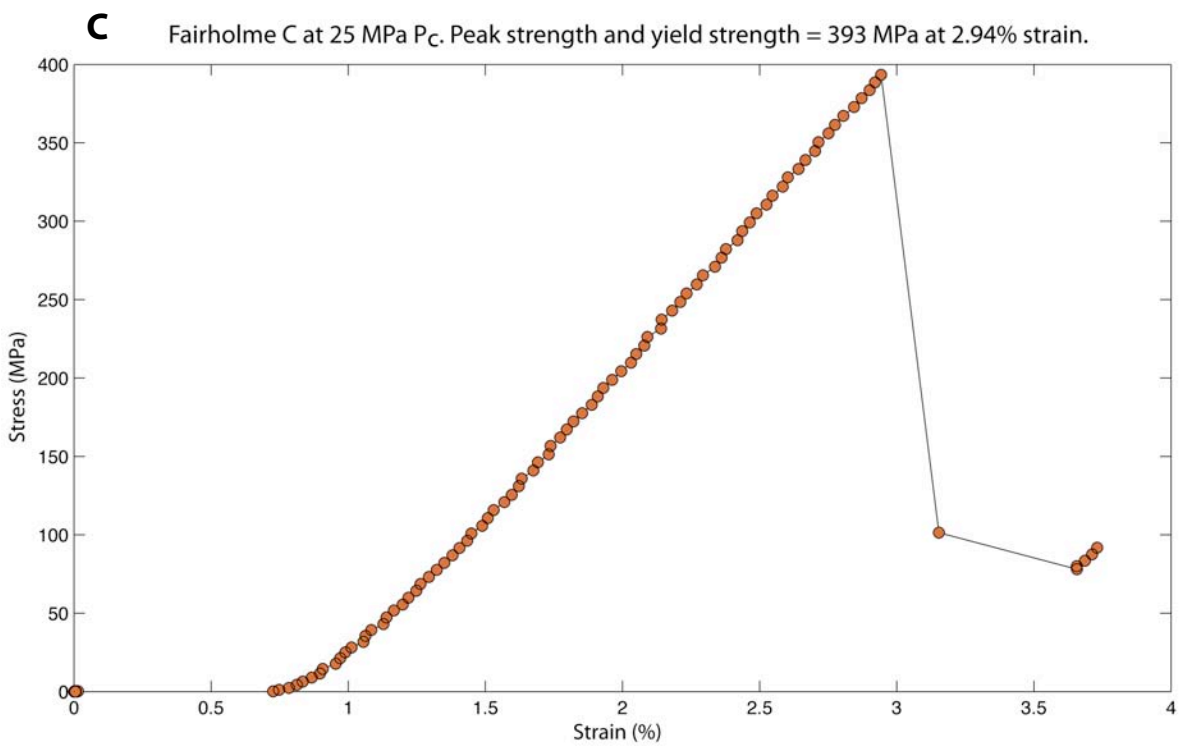

Figure 4 *cont.* - C. Stress-strain curve for Fairholme C at $P_c = 25$ MPa.

Loomis 3 Deformation

The Loomis 3 member is a bioclastic limestone with a micritic matrix (Figure 5). The primary fracture surface is highly irregular with comminuted gouge and fragments of wall rock contained within the fracture. Strain within the sample appears to be well distributed as cracks are present throughout the rock. Mode I cracks are present parallel to σ_1, proximal to the primary fracture surface. Multiple pathways exist in the direction of the primary fracture. potentially enhancing fluid flow.

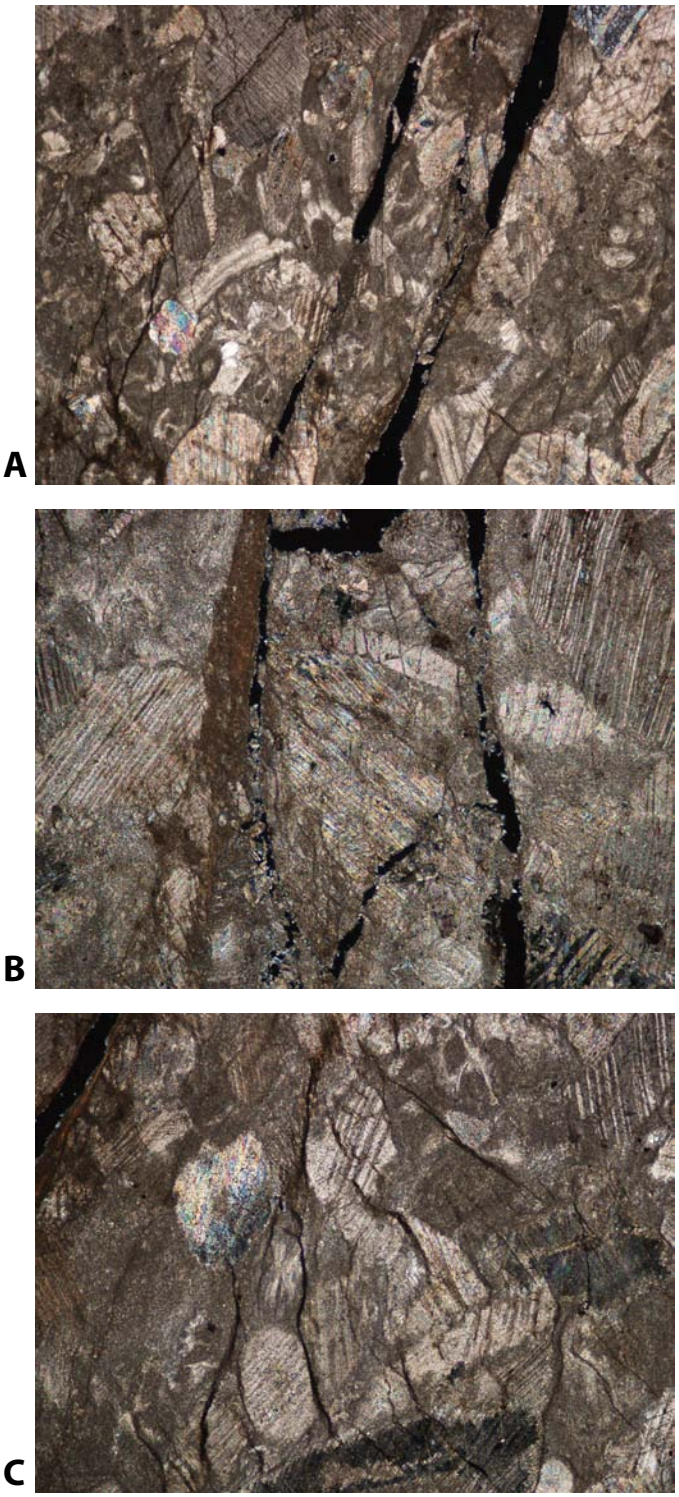

Figure 5. Loomis 3 limestone photomicrographs. All images are in cross polarized light. **A.** *Field of view: 3.9 mm.* Multiple fractures form the primary shear zone. **B.** *Field of view: 2.0 mm.* Detail of wall rock fragment contained within the primary fracture. Comminuted gouge left of center along wall rock. **C.** *Field of view: 2.0 mm.* Vertical Mode I cracks are aligned parallel to σ_1. Fracture visible in top left of section.

Baril Wileman 83 Deformation

The Baril Wileman 83 sample is a calcitic dolostone with angular grain boundaries (Figure 6). The primary fracture is non-planar and irregular, though less so than the Loomis 3 fracture. This rock was the most porous of the sample suite which is observable as well distributed vugs throughout the sample. Highly comminuted gouge material is still present along the fracture wall in some areas. Distribution of strain appears to be limited to the primary fracture surface with no other structures related to the triaxial deformation present.

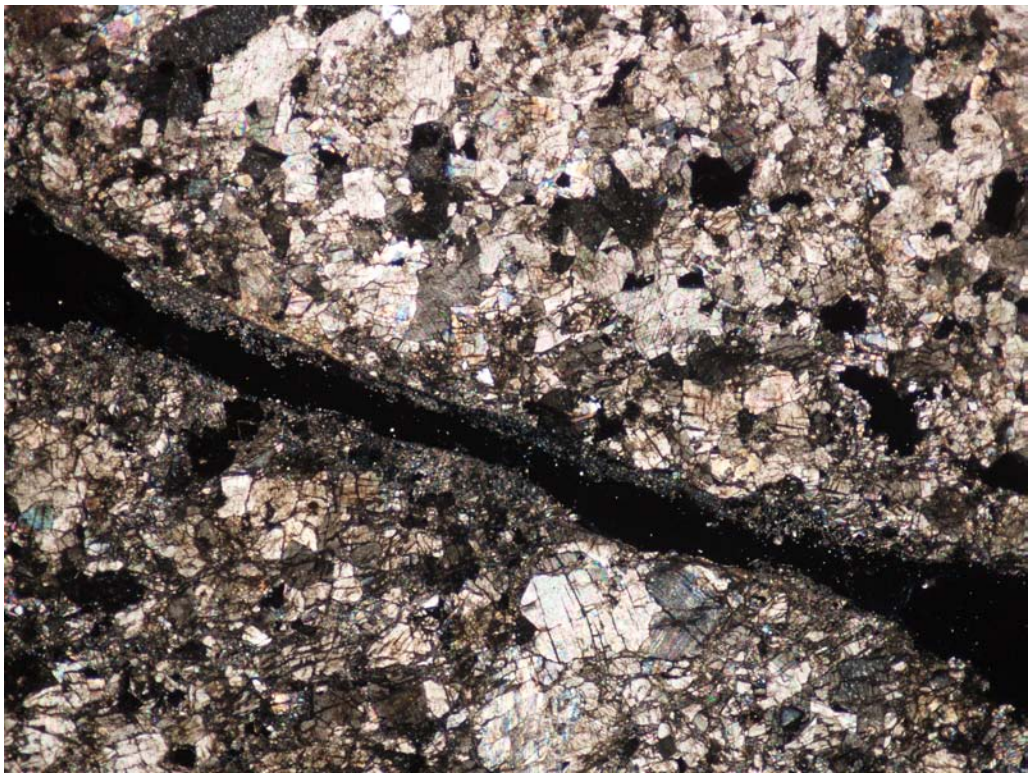

Figure 6. Baril Wileman 83 calcitic dolostone photomicrograph in cross polarized light. *Field of view: 3.9 mm.* Irregular fracture surface with variable thickness. Highly comminuted gouge lines edge of fracture. Opaque black areas mark vuggy porosity.

Fairholme C Deformation

Fairholme C is a nearly pure dolostone with the highest strength of the rocks tested (Figure 7). The primary fracture surface is irregular, with variations in thickness along its entire extent. As in the Baril Wileman member, very little distributed strain is expressed outside of the primary fracture. The gouge produced in the deformation is highly

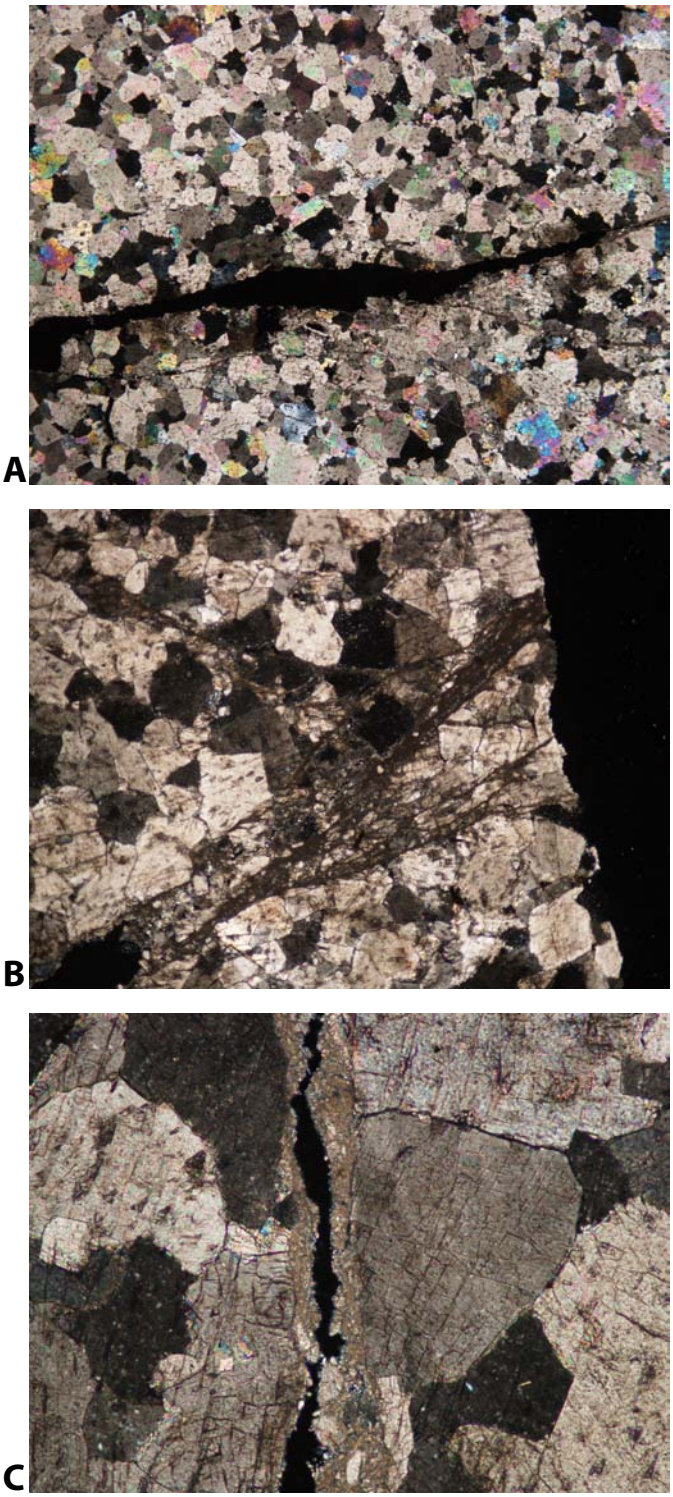

Figure 7. Fairholme C dolostone photomicrographs. All images in cross polarized light. **A.** *Field of view: 3.9 mm.* Irregular fracture surface showing very little gouge remaining along fracture walls. Strain is limited to the shear zone. **B.** *Field of view: 3.9 mm.* Fracture surface that has not experienced fluid flow. Scoured fracture can be seen in extreme bottom left. Fluid port is located into the page. **C.** *Field of view: 2.0 mm.* Detail of irregular fracture surface with highly comminuted gouge lining wall rock.

comminuted, with grain sizes beyond the power of the optical microscopes used. Though most of the gouge appears to have been scoured from the fracture, an area suspected to be above the fluid flow port shows a tight network of fractures and gouge material. This is likely a segment of the original undisturbed fracture surface prior to fluid flow. This fine grained comminution, with little other fracturing is expected to not enhance permeability of the sample.

Permeability Results

A number of attempts were made to determine the permeability of the deformed samples. Of these attempts, usable data was obtained from two, the Baril Wileman 83 and Fairholme C cores. It must be noted that these decay curves were taken from the period of building up pressure for higher pressure pulse decay tests, therefore the upper reservoir was not isolated during the increase in pressure. The upper reservoir volume was determined by subtracting the lower reservoir volume from the pump volume. Using the mathematical model described above, the upper fluid reservoir pressure decay curves were plotted and fitted with both robust and non-robust exponential curves (Figure 8).

Both the non-robust and robust exponential coefficients were used for α values. The mean permeability was calculated from both α derived permeabilities. Calculations from the model result in a slightly higher permeability for the more calcite-rich Baril Wileman 83 sample than the nearly pure dolomite Fairholme C sample (Table 4).

Table 4. Measured fracture permeability values.

Sample	Pressure - *MPa*				α - 10^{-3} s^{-1}		Average k - 10^{-17} m^2
	P_s	P_f	P_c	ΔP	Non-robust	Robust	
Baril Wileman 83	2.75	1.95	5	0.8	8.83	8.89	**7.69**
Fairholme C	1.8	0.33	5	1.6	9.43	5.45	**4.36**

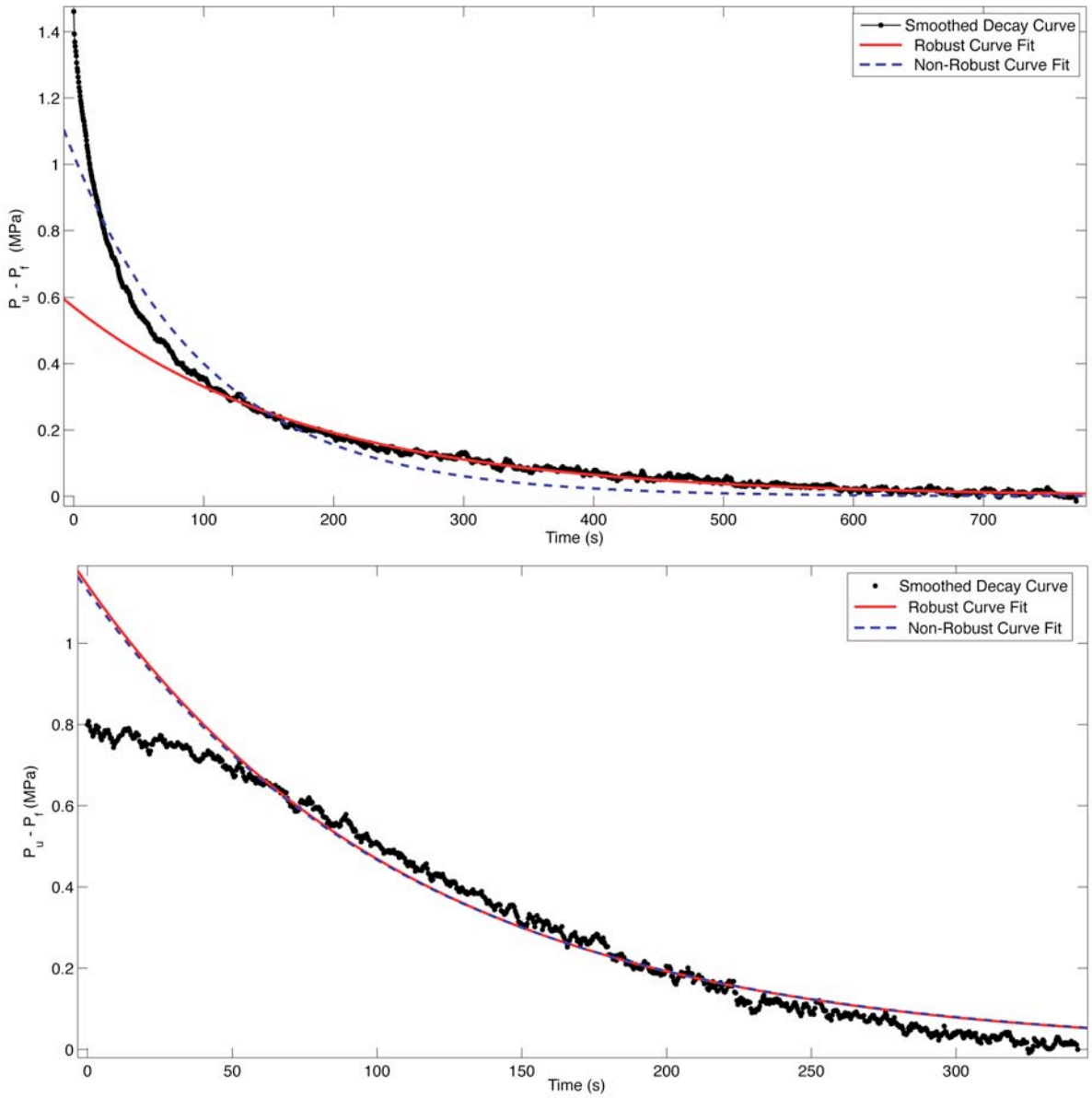

Figure 8. A. Transient pulse decay and exponential models for Fairholme C sample. **B.** Transient pulse decay and exponential models for Baril Wileman 83 sample.

DISCUSSION

The scope of this experimentation was to develop a methodology for determining permeability using the transient pulse decay method with the equipment available at UBC-CESL and to investigate the role of dolomite in the permeability of fracture surfaces in

limestone-dolomite composite rocks. Preliminary results presented above mark a significant benchmark for similar permeability studies in the future.

Permeability

The simplest comparison that can be made is the Baril Wileman 83% dolomite fracture surface is more permeable than the nearly pure Fairholme C 99% dolomite sample. This result could be attributable to the bimineralic nature of the Baril Wileman caused by the increased amount of calcite. The difference in strength of calcite and dolomite is demonstrated in the deformation tests above and in Cleven (2008). Gouge produced in limestone-dolomite composite fractures would be expected to have a wider distribution of grain sizes, potentially allowing greater fluid flow where as highly concentrated strain in monomineralic end members results in a very fine homogeneous gouge that acts to inhibit fluid flow. Though no successful permeabilities were calculated for the Loomis 3 sample, the increased heterogeneity and Mode I cracks of that rock would be expected to increase permeability of the fracture surface. The much larger damage zone as seen in the thin section of the Loomis 3 could be a zone of enhanced permeability (Figure 9).

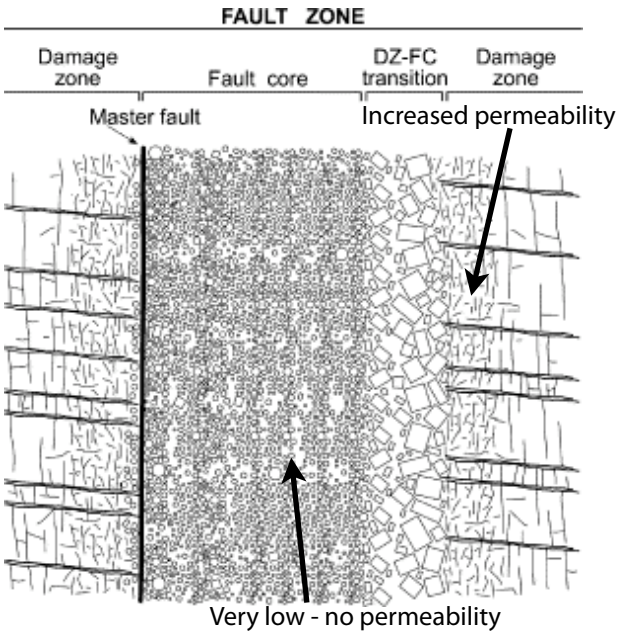

Figure 9. Conceptual cross section of fault zone perpendicular to shear direction illustrating differences between cataclastic core gouge and fault damage zone (modified from Billi et al, 2003).

Microstructural analysis of the fracture surfaces shows that all of the induced fractures are highly irregular in nature with variable widths along the lateral extent of the fracture. Permeability is a function of the cross sectional area through which a fluid is flowing through as stated by Darcy's Law (eq. 1). Narrower segments in the primary fracture will limit the permeability of the fracture as the area of the fracture is reduced. Increasing the heterogeneity of a rock appears to result in the generation of multiple fractures along which permeability could be enhanced. However, measurements of permeability are made with the rock experiencing a confining pressure. This confining pressure acts to close the fractures, but whether or not this occurs or if the fluid pressure that acts against the confining pressure props open the fracture is not known and is a matter for further research. If the effects of confining pressure, or differential pressure are significant, this will effect the choice of experimental conditions and the models used to interpret the decay curves.

The permeability measurements conducted for this research were calculated from data collected during the buildup of pressure to the original desired experimental conditions of 25 MPa of confining pressure and 20 MPa of fluid pressure. The process of building up fluid pressure in the sample is suspected to cause failure of the annular seal between the polyolefin jacket and the sample wall. In addition, gouge material is believed to have been extruded during the application of fluid pressure in some experiments as seen when the system was emptied. This is also suggested by the nearly empty fracture surface seen in thin section. The original fracture prior to fluid flow within the sample may be seen in figure 7B. Modification of the fracture core gouge suggests a need for improved control in maintaining gouge so that measurements are performed on undisturbed gouge.

Due to a lack of successful permeability experiments, it is difficult to make explicit comparisons between the two successful tests. However, permeability data listed by Wibberley & Shimamoto (2002) for natural fault gouges from the San Andreas, Carboneras and Nojima faults show values of 10^{-18} to 10^{-22} m^2, the minimum being one order of magnitude less than the results achieved with experimentally induced carbonate gouge in this study.

The process of permeability modeling in this study is a modified version of Brace et al (1968). This model excludes storage within the sample, which is a reasonable assumption for the very low porosity of most rocks in the sample suite. Storage can be accounted for using the improved mathematical models developed for the transient pulse method (eg. Hsieh et al., 1981, Kamath et al., 1992, Zeynaly-Andabily & Rahman 1995, etc.).

Explicit values for error in the permeability values have not been calculated. The results are therefore suggested to be interpreted at a logarithmic unit scale, with these permeabilities being about -17 m^2 in log units. Further research is planned to improve these results and provide more accurate values for permeability.

Troubleshooting

Though the methods for determining permeability of tight rocks are simple on paper, there are many difficulties in achieving a successful experiment. The number of steps in the experimental process is a major vulnerability. Each sample is only usable once due to the redistribution and elimination of gouge material when the pore fluid pressure is applied to the sample. This makes it necessary to prepare each sample with extreme care. A silicone adhesive was used to affix the polyolefin jacket to the rock sample but the effectiveness of this seal is questionable at higher fluid pressures. Annular space seal integrity is essential as any diversion of fluid away from the sample results in virtually unusable data. Unfortunately, this was a more common occurrence than desired. Alternatives to the silicone adhesive might include using an annealed copper jacket to ensure fluid flow is directed through the sample. The pore fluid pressure oscillation method can be used to help negate the effects of small leaks, but this requires the use of volumometers.

The redistribution and loss of gouge material is something to be considered in future experimental design. Measuring the true permeability of a fault core gouge could be made difficult if gouge is significantly affected each time a measurement is attempted. Elimination of gouge might be prevented or at the very least reduced by using a ceramic packed drill port as used by Crawford et al (2008). Application of a higher confining pressure from the beginning of a test might also alleviate this problem. That would affect the permeability of

the sample as cracks and the primary fracture are reduced in size but this could be accounted for and the benefits of undisturbed gouge would be great.

Another issue arose with the drill hole ports. Though the ports were made using a precision milling machine, the distance to drill was determined by estimating where the fracture surface would intersect the drill hole. If the drill hole for some reason did not intersect the fracture equilibration of the upper and lower reservoirs would not happen. An experiment where this situation occurred was left with fluid pressure applied in the upper reservoir with the expectation of equilibrium being reached but no change in the lower reservoir transducer was noted over the course of seven hours.

CONCLUSION

A method for the determination of permeability of experimentally induced fracture surfaces has been developed for the facilities at UBC-CESL. This involves utilizing the frequently used transient pulse decay method on rocks prepared for fluid flow along the primary fracture caused by a triaxial compression test. This method has been applied to a suite of limestone-dolomite composite rocks successfully in two cases. These permeabilities are within or near known theoretical and experimental values of permeability derived for fault cores and gouge materials. With further refinements of technique and modeling, this study serves as a significant initial benchmark for the study of permeability of deformed rocks and will act to guide future researchers. The permeability characterization of these fracture surfaces should be of assistance to researchers looking at limestone-dolomite hosted fault rocks.

ACKNOWLEDGEMENTS

First and foremost, I would like to thank Dr. Lori Kennedy for allowing me to work in the lab and providing constant support for the past seven months. Without her this study would be impossible. I'd like to thank Dr. Kelly Russell for the pep talks and advice along the way. Mr. Doug Polson was instrumental in many of the technical aspects and I am indebted to him for drilling the sample fluid ports, even on short notice. Dr. Mary Lou Bevier coordinated and organized the course structure and her clear guidelines and expectations have provided great guidance. Dr. Greg Dipple provided advice on rock transport properties and his time was greatly appreciated. Dr. Stephen Cox of Australia National University visited UBC and in the process of touring CESL, provided me with greatly appreciated advice and motivation. When he said these experiments are very hard, he meant it. Mr. Nathan Cleven, though he and I never crossed paths, put a very large effort into his undergraduate thesis last year and it was his cores and data that sparked this project. Lastly, I'd like to thank my fellow classmates and friends for their support as they have endured many a rant in the past several months.

REFERENCES

Austin, N.J., 2003, An experimental investigation of textural controls on the brittle deformation of dolomite [M.Sc. dissertation], Vancouver, University of British Columbia, 95 p.

Billi, A., Salvini, F., and Stortini, F., 2003, The damage zone-fault core transition in carbonate rocks: implications for fault growth, structure and permeability, Journal of Structural Geology, v. 25, 1779-1794.

Brace, W.F., Walsh, J.B., and Frangos, W.T., 1968, Permeability of granite under high pressure, Journal of Geophysical Research, v. 73, 2225-2236.

Cleven, N.R., 2008, The role of dolomite content on the mechanical strength and failure mechanisms in dolomite-limestone composites [B.Sc. dissertation], Vancouver, University of British Columbia, 70 p.

Crawford, B.R., Faulkner, D.R., and Rutter, E.H., 2008, Strength, porosity, and permeability development during hydrostatic and shear loading of synthetic quartz-clay fault gouge, Journal of Geophysical Research, v. 113, B03207.

Ehrenberg, S.N., Eberli, G.P., Keramati, M., and Moallemi, S.A., 2006, Porosity-permeability relationships in interlayered limestone-dolostone reservoirs, American Association of Petroleum Geologists Bulletin, v. 90, 91-114.

Faulkner, D.R. and Rutter, E.H., 2000, Comparisons of water and argon permeability in natural clay-bearing fault gouge under high pressure at 20°C, Journal of Geophysical Research, v. 105, B7, 16415-16426.

Fischer, G.J., 1992, The determination of permeability and storage capacity: Pore pressure oscillation method, In: Evans, B. and Wong, T-F., editors, Fault Mechanics and Transport Properties of Rocks, London, Academic Press, p. 187-212.

Giger, S.B., 2007, Permeability and strength evolution of quartz fault gouges at hydrothermal conditions [Ph.D. dissertation], Canberra, Australia National University, 125 p.

Hsieh, P.A., Tracy J.V., Neuzil, C.E., Bredehoeft, J.D., and Silliman, S.E., 1981, Transient laboratory method for determining the hydraulic properties of ‘tight’ rocks - I. Theory, International Journal of Rock Mechanics and Mining Science & Geomechanics Abstracts, v. 18, 245-252.

Kamath, J., Boyer, R.E., and Nakagawa, F.M., 1992, Characterization of core-scale heterogeneities using laboratory pressure transients, Society of Petroleum Engineers Formation Evaluation, v. 7, 219-227.

Monaco, C., Mazzoli, S., and Tortorici, L., 1996, Active thrust tectonics in western Sicily (southern Italy): the 1968 Belice earthquake sequence, Terra Nova, v. 8, 372-381.

Pace, B., Boncio, P., and Lavecchia, G., 2002, The 1984 Abruzzo earthquake (Italy): an example of seismogenic process controlled by interaction between differently oriented synkinematic faults, Tectonophysics, v. 350, 237-254.

Wibberley, C.A.J., and Shimamoto, T., 2002, Internal structure and permeability of major strike-slip fault zones: the Median Tectonic Line in Mie Prefecture, Southwest Japan, Journal of Structural Geology, v. 25, 59-78.

Zeynaly-Andabily, E.M. and Rahman, S.S., 1995, Measurement of permeability of tight rocks, Measurement Science and Technology, v. 6, 1519-1527.

Zhang, M., Takahashi, M., Morin, R. H., and Esaki, T., 2000, Evaluation and application of the transient-pulse technique for determining the hydraulic properties of low-permeability rocks—Part 1: theoretical evaluation, Geotechnical Testing Journal, v. 23, 83–90.

Zhang, M., Takahashi, M., Morin, R. H., and Esaki, T., 2000, Evaluation and application of the transient-pulse technique for determining the hydraulic properties of low-permeability rocks—Part 2: experimental application, Geotechnical Testing Journal, v. 23, 91–99.

APPENDIX

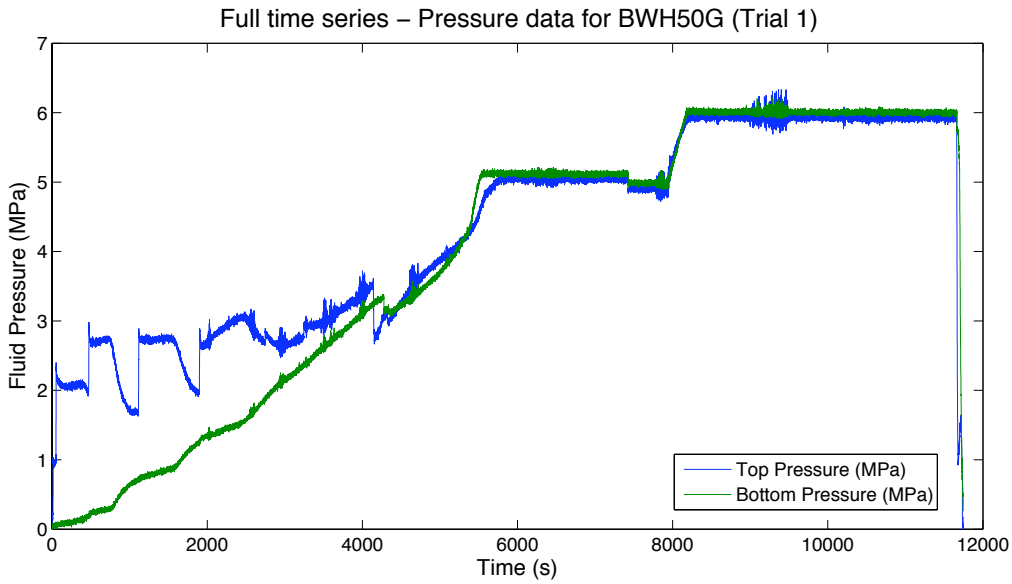

Figure 10. Unedited time series of upper and lower reservoir pressures for Baril Wileman 83 sample. At time ~6000 seconds, reservoirs reach equilibrium, but it appears the annular seal was broken at that point, resulting in unusable data following that point.